

1 **Understanding the Australian Monsoon change during the Last Glacial Maximum**
2 **with multi-model ensemble**

3 **Mi Yan^{1,2}, Bin Wang^{3,4}, Jian Liu^{1,2*}, Axing Zhu^{1,2,5,6}, Liang Ning^{1,2,7} and Jian Cao⁴**

4 1 Key Laboratory of Virtual Geographic Environment, Ministry of Education; State key
5 Laboratory of Geographical Environment Evolution, Jiangsu Provincial Cultivation Base; School
6 of Geography Science, Nanjing Normal University, Nanjing, 210023, China.

7 2 Jiangsu Center for Collaborative Innovation in Geographical Information Resource
8 Development and Application, Nanjing, 210023, China.

9 3 Department of Atmospheric Sciences, University of Hawaii at Manoa, Honolulu, HI 96825,
10 USA.

11 4 Earth System Modeling Center, Nanjing University of Information Science and Technology,
12 Nanjing, 210044, China.

13 5 State Key Lab of Resources and Environmental Information System, Institute of Geographic
14 Sciences and Natural Resources Research, Chinese Academy of Sciences, Beijing, 100101,
15 China

16 6 Department of Geography, University of Wisconsin-Madison, Madison, WI 53706, USA

17 7 Climate System Research Center, Department of Geosciences, University of Massachusetts,
18 Amherst, 01003, USA.

19
20 * Corresponding author address: Dr. Jian Liu, School of Geography Science, Nanjing Normal
21 University, 1 Wenyuan Road, Nanjing 210023, China

22 E-mail: jliu@njnu.edu.cn

Abstract

The response of Australian monsoon to the external forcings and the related mechanisms during the Last Glacial Maximum (LGM) is investigated by multi-models' experiments in CMIP5/PMIP3. Although the annual mean precipitation over the Australian monsoon region decreases, the annual range, or the monsoonality, is enhanced. The precipitation increases in early austral summer and decreases in austral winter, resulting in the amplified annual range, but the main contribution comes from the decreased precipitation in austral winter. The decreased winter precipitation is primarily caused by weakened upward motion, although reduced water vapor has also a moderate contribution. The weakened upward motion is induced by the enhanced land–sea thermal contrast, which intensifies the divergence over the northern Australia. The increased Australian monsoon rainfall in early summer, on the other hand, is an integrated result of the positive effect of local dynamic processes (enhanced moisture convergence) and the negative effect of thermodynamics (reduced moisture content). The enhanced moisture convergence is caused by two factors: the strengthened northwest–southeast thermal contrast between the cooler Indochina–western Indonesia and the warmer northeastern Australia, and the east–west sea surface temperature gradients between the warmer western Pacific and cooler eastern Indian Ocean, both due to the alteration of land–sea configuration arising from the sea level drop. The enhanced Australian monsoonality in the LGM is not associated with global scale circulation change such as the shift of the ITCZ, rather, it is mainly due to the change of regional circulations around Australia arising from the changes in land-sea contrast and the east-west SST gradients over the Indo-western Pacific oceans. This finding should be taken into account when investigating its future change under global warming. Our findings may also explain why proxy records indicate different changes in Australian monsoon precipitation during the LGM.

49 **1 Introduction**

50 The changes of the Australian monsoon are crucial for human society and ecology in
51 Australia (Reeves et al., 2013a), considering the socio-economic importance of monsoon rainfall
52 (Wang et al., 2017). As the monsoons of the summer hemisphere are linked via outflows from
53 the opposing winter hemisphere, the Australian monsoon can also influence the Asian–
54 Indonesian–Australian monsoon system (Eroglu et al., 2016). It is important to understand how
55 and why the Australian monsoon would change in response to global climate change.

56 With strong climatic forcings (including low greenhouse gas (GHG) concentrations, large
57 ice-sheets, and low sea level, etc.), the Last Glacial Maximum (LGM) is one of the key periods
58 that provides an opportunity to better understand the mechanisms of how global and regional
59 climate respond to external forcings (Hewitt et al., 2001; Braconnot et al., 2007; Braconnot et al.,
60 2011; Harrison et al., 2014). Previous studies have investigated how the external forcing and
61 boundary conditions during the LGM affected the Intertropical Convergence Zone (ITCZ)
62 (Broccoli et al., 2006; Donohoe et al., 2013; McGee et al., 2014), the Walker circulation
63 (DiNezio et al., 2011), the Indo-Pacific climate (Xu et al., 2010; DiNezio and Tierney, 2013;
64 DiNezio et al., 2016), the SH circulation (Rojas, 2013), and the global monsoon (Jiang et al.,
65 2015; Yan et al., 2016). The Australian monsoon onset and variability during the post-glacial, the
66 late deglaciation, and the Holocene have also been studied using proxy datasets (Ayliffe et al.,
67 2013; De Deckker et al., 2014; Kuhnt et al., 2015; Bayon et al., 2017). However, due to the
68 limitation of the scarce proxy datasets, the Australian monsoon change during the LGM is far
69 from clearly understood.

70 There are different proxy evidences indicating different Australian monsoon change
71 during the LGM. Here, the Australian monsoon intensity is represented by the seasonality of
72 precipitation, i.e., a stronger monsoon means a wetter summer and/or drier winter. Some records
73 show wet conditions over Australia during the LGM (Ayliffe et al., 2013), while other proxies
74 indicate drier conditions (Denniston et al., 2013; Denniston et al., 2017; DiNezio and Tierney,
75 2013). The isotopes from eggshell of five regions across Australia affirms that Australia becomes
76 drier in the LGM (Miller et al., 2016), while the archaeological record showed a refugia-type
77 hunter-gatherer response over northwest and northeast Australia during the LGM (Williams et
78 al., 2013), indicating that these areas may have had a wetter summer and were therefore

79 preferred by people as refugia. The synthesis by the OZ-INTIMATE (Australian INTIMATE,
80 INTegration of Ice core, MARine and TERrestrial records) project (Turney et al., 2006; Petherick
81 et al., 2013) showed that the palaeoenvironment over Northern Australia during the LGM was
82 characterized by drier conditions although wet periods were also noted in the fluvial records
83 (Reeves et al., 2013a; Reeves et al., 2013b).

84 The change in the Australian monsoon was inconclusive during the LGM based on proxy
85 data. Therefore, scholars started investigating the Australian monsoon change from numerical
86 simulation perspectives. The sensitivity of Australian monsoon to forcings during the late
87 Quaternary has been analyzed using simulations by Fast Ocean Atmosphere Model (Marshall
88 and Lynch, 2006, 2008). Numerical experiments have been conducted to analyze the impacts of
89 obliquity and precession with a coupled General Circulation Model (Wyrwoll et al., 2007) and
90 orbital time-scale circulation with Community Climate Model (Wyrwoll et al., 2012) on the
91 Australian monsoon. However, different models may have different responses to the same
92 external forcings, such that the simulated results may have model dependence. Multi-model
93 ensemble (MME) can reduce the model biases and therefore provide more reasonable results of
94 how and why climate system responds to the external forcing changes. The MME can also
95 provide a clearer perspective on model uncertainties.

96 Yan et al (2016) thus used the multi-model ensemble approach to examine the response
97 of global monsoon to the LGM conditions. It was found that the global monsoon and most sub-
98 monsoons weakened under the LGM conditions. Some brief hypothesis was made to explain the
99 changes from global and hemispheric perspectives. The Australian monsoon was thought to be
100 strengthened due to the southward shift of the ITCZ resulted from the hemispheric thermal
101 contrast and due to the land-sea thermal contrast resulted from the land-configuration. However,
102 this simulated result of strengthened monsoon or wet condition has not been proved yet. As
103 mentioned above, it is inconclusive whether the Australian monsoon is strengthened or not
104 during the LGM, due to the limitations of proxies' and models' uncertainties. Neither model
105 outputs nor proxy records provide a "true" record of the LGM, as proxy records require
106 interpretation and calibration and may be spatially incomplete, while models contain biases.
107 Therefore, model-data and inter-model comparison are needed and studies on the mechanisms
108 are required to better understand the Australian monsoon change during the LGM. Moreover,
109 some studies show that the Australian climate during the last glacial period was modulated by

110 additional mechanisms rather than simply the ITCZ (Bayon et al., 2017). Thus, single forcing
111 runs are also required to figure out the contributions of different forcings.

112 This paper investigates the Australian monsoon change during the LGM and its
113 mechanisms from both thermodynamics and dynamics perspectives, using the multi-model
114 ensemble mean derived from models in the fifth phase of the Coupled Model Intercomparison
115 Project (CMIP5) (Taylor et al., 2012) and the third phase of the Paleoclimate Modeling
116 Intercomparison Project (PMIP3) (Braconnot et al., 2012). We are also trying to quantify the
117 contributions of the thermodynamic and the dynamic processes to the Australian monsoon
118 change during the LGM. Additionally, we are applying single forcing run to test the effect of
119 land-configuration as mentioned in Yan et al. (2016). The models and experiments used in this
120 paper are introduced in Sect. 2. Section 3 describes simulated results and the physical
121 mechanisms. The comparison with proxies and other simulations is discussed in Sect. 4 and the
122 conclusions are made in Sect. 5.

123

124 **2 Methods**

125 2.1 Model and experiments

126 Two experiments performed by models participating in CMIP5/PMIP3 are compared in
127 this paper: the Last Glacial Maximum Experiment (LGME) and the pre-industrial (PI) control
128 run (piControl). The models and experiments are listed in Table 1, including 7 models and 2
129 experiments. The models contributed to CMIP5 have been evaluated in the previous studies to
130 have good performance in simulating the Australian monsoon precipitation seasonality or
131 seasonal cycle (Jourdain et al., 2013; Brown et al., 2016), which is used to represent the
132 Australian monsoon intensity in this study.

133 The last 100 years of the LGME and the last 500 years of the piControl from each model
134 are used to illustrate the model climatology. To obtain the multi-model ensemble (MME), the
135 model outputs were interpolated into a fixed 2.5° (latitude) \times 2.5° (longitude) grid using the
136 bilinear interpolation method.

137 The LGM external forcing and boundary conditions are listed in Table 2. More specific
138 documentation can be found on the PMIP3 website (<https://pmip3.lscce.ipsl.fr>). Compared with

139 the PI, during the LGM the Southern Hemisphere (SH) low latitudes (30°S-EQ) receive more
 140 insolation from January to August and less from August to December. The NH low latitudes
 141 (EQ-30°N) receive less insolation from June to October and more from November to May (Fig.
 142 S1). Due to the decreased sea level, the landmasses expanded during the LGM. A land bridge
 143 formed between Indochina and western Indonesia, and the Arafura Sea between New Guinea and
 144 Australia closed and became landmass (Fig. S2).

145 To illustrate the robust changes simulated by the different models, the signal-to-noise
 146 ratio (S2N) test is used. The S2N is defined by the ratio of the absolute mean of the MME (as the
 147 signal) to the averaged absolute deviation of the individual model against the MME (as the
 148 noise) (Yan et al., 2016). In the following sections, we only consider the areas in which the S2N
 149 ratio exceeds one when we examine the differences between the LGME and piControl derived
 150 from the MME.

151 2.2 Decomposition method

152 For attribution of precipitation changes, we use a simplified relation based on the
 153 linearized equation of moisture budget used in the previous works (Chou et al., 2009; Seager et
 154 al., 2010; Huang et al., 2013; Endo and Kitoh, 2014; Liu et al., 2016). Considering a quasi-
 155 equilibrium state, the vertical integrated moisture conservation can be written as:

$$156 \quad - \int_{1000}^0 \nabla \cdot (q \vec{v}) dp = P - E \quad (1)$$

157 where q is specific humidity, \vec{v} is horizontal velocity, p is pressure, P is precipitation, and E the
 158 surface evaporation. Since water vapor is concentrated in the lower troposphere, the vertical
 159 integrated total column moisture divergence can be approximately replaced by the integration
 160 from the surface to 500 hPa. Define the $\Delta(\cdot)$ as the change from PI to the LGM, i.e.,

$$161 \quad \Delta(\cdot) = (\cdot)_{\text{LGM}} - (\cdot)_{\text{PI}} \quad (2)$$

162 Then the precipitation change ΔP can be calculated as follows:

$$163 \quad \Delta P = - \int_{p_{1000}}^{p_{500}} \Delta(q \cdot \nabla \vec{v}) dp - \int_{p_{1000}}^{p_{500}} \Delta(\vec{v} \cdot \nabla q) dp + \Delta E \quad (3)$$

164 To further simplify the equation, we use $-\omega_{500}$ to represent vertical integrated $\nabla \vec{v}$, and q at the
 165 surface to represent vertical integrated specific humidity (Huang et al., 2013). Thus, the
 166 precipitation change (ΔP) can be represented as

$$167 \quad \Delta P \propto \bar{\omega}_{500} \cdot \Delta q + \bar{q} \cdot \Delta \omega_{500} + \Delta E - \Delta T_{adv} \quad (4)$$

168 where $\bar{\omega}_{500}$ is 500 hPa vertical velocity in PI, \bar{q} is surface specific humidity in PI, ΔT_{adv} is the
169 changes due to the moisture advection ($\int_{p_0}^{p_{500}} \Delta(\vec{v} \cdot \nabla q) dp$).

170 The first term in the right-hand side of (4) ($\bar{\omega}_{500} \cdot \Delta q$) represents thermodynamic effect (due to
171 the change of q), and the second term ($\bar{q} \cdot \Delta \omega_{500}$) represents dynamic effect (due to the change of
172 circulation).

173 2.3 Monsoon domain

174 The monsoon domain is defined following hydroclimate definition, i.e., a contrast
175 between wet summer and dry winter (Wang and Ding 2008). The monsoon domain is defined by
176 the area where the annual range (local summer minus local winter) exceeds 2.0 mm/day, and the
177 local summer precipitation exceeds 55% of the annual total precipitation. Here in the southern
178 hemisphere, summer means November to March and winter means May to September. Since the
179 domains derived from different models are different, and the changes of domain are also
180 different, we use the fixed domain derived from the merged Climate Prediction Center Analysis
181 of Precipitation (CMAP, Xie and Arkin, 1997) and Global Precipitation Climatology Project
182 (GPCP, Huffman et al., 2009) data.

183 Note that the monsoon domain is shown to give a general view of precipitation change,
184 but not the purpose of this study.

185

186 3 Results

187 We defined the difference of precipitation rate between austral summer (DJF) and austral
188 winter (JJA) as the annual range, i.e. the seasonality, to measure the monsoonality of the
189 Australian monsoon. An increased annual range (or seasonality) means a strengthened
190 monsoonality. Unlike the South African and South American monsoon regions (not shown), the
191 monsoonality of the Australian monsoon derived from the seven models' multi-model ensemble
192 (7MME) is strengthened during the LGM (Fig. 1a). This amplified annual range is the result of
193 increased precipitation in austral summer and decreased precipitation in austral winter (Fig. 1b).
194 Note that the largest decrease in precipitation occurred from April to July (late autumn to early
195 winter), not exactly in austral winter; and the largest increase of precipitation occurred in
196 November and December (ND), i.e., austral early summer. Since the amount of autumn–winter

197 reduction of precipitation exceeds the increased precipitation in early summer, the annual mean
198 precipitation over the strengthened annual range region decreases (by 0.36 mm/day). In
199 summary, while the total annual precipitation decreases in the LGM, the annual range (or the
200 seasonality) of the Australian monsoon rainfall is amplified due to seasonal redistribution of the
201 precipitation, especially the drying in austral autumn (April–May) and winter (JJA) over
202 Australia.

203 Although there are model biases, most of the models (except MPI-ESM-P) simulate an
204 enhanced annual range (or seasonality/monsoonality) in the central Australian monsoon region
205 (20°S–5°S, 120°E–145°E) (Table 3 and Fig. 1c). Most of the models (except CNRM-CM5 and
206 MPI-ESM-P) also simulate an increased summer precipitation over that region. All the models
207 simulate decreased precipitation from April to September (Fig. 1c). On the other hand, the
208 simulated annual mean precipitation is decreased in most models, except GISS-E2-R. The model
209 uncertainties will be discussed later in Sec. 4.

210 3.1 Reasons for the decreased precipitation during the LGM in austral winter (JJA)

211 During the LGM, the lower GHG concentration and the large ice-sheets are the primary
212 causes for the decreased global temperature and the humidity. The global surface specific
213 humidity is reduced by 2 g/kg (or 20 %) in JJA during the LGM, compared with the PI. For the
214 SH monsoon regions, the surface specific humidity is reduced more over the Australian monsoon
215 region than over the other two monsoon regions of South Africa and South America (Fig. 2).

216 As suggested by the Clausius–Clapeyron relation (C-C relation), one degree of
217 temperature decrease would lead to about a 7 % decrease in the saturation water vapor (Held and
218 Soden, 2006), or roughly the same scale of decrease in the low tropospheric specific humidity. If
219 the circulation, evaporation and advection remains unchanged, the precipitation should also be
220 reduced by 7 % with regard to the equation (4). During the LGM, the simulated near surface air
221 temperature over the central Australian monsoon region (20°S–5°S, 120°E–145°E) decreases
222 significantly by 2.5 K in JJA, which implies a decrease of about 17 % resulted from the C-C
223 relation. However, the simulated precipitation in the LGM is reduced by 1.45 mm/day or 44 %
224 comparing to the PI, which is far beyond the value suggested by the thermodynamic effect
225 (approximately 17 %). This suggests that the majority of the reduction in winter precipitation is
226 due to the changes of rest terms in equation (4), including the circulation change (dynamics), the

227 evaporation change and the change due to the advection term. The changes of each terms show
228 that the circulation change plays a dominant role in the precipitation change over Australia (Fig.
229 S3). The change due to the evaporation is also important. The change due to the advection term
230 is negligible.

231 The change of the surface wind field shows a strengthened divergence pattern over the
232 Australian monsoon region (Fig. 3a, vector), which is consistent with the strengthened
233 descending flow over the Australian monsoon region (Fig. 4) and thus reduced precipitation (Fig.
234 3a, shading). The JJA mean near surface air temperature shows that the land is cooler than the
235 adjacent ocean around northern Australia (Fig. 5a), which illustrates a strengthened land–sea
236 thermal contrast because the land cools more than the ocean surface during the LGM. This
237 strengthened land–sea contrast leads to a higher sea-level pressure (SLP) over land and lower
238 SLP over ocean in general (Fig. 5b, shading), and thus the outflows from land (Fig. 5b, vector).
239 The geopotential height at 850 hPa also shows the relative pattern that matches the wind change
240 (Fig. S4a). The difference of divergence/convergence field (Fig. 5c) also indicates that the
241 divergence at 850 hPa over the northern Australia is strengthened during the LGM. The vertical
242 velocity at 500 hPa over the central Australian monsoon region (20°S-5°S, 120°E-145°E)
243 illustrates that the descending flow strengthened by about 48 %.

244 In conclusion, both the dynamic process (increased subsidence) and the thermodynamic
245 process (reduced water vapor content) contribute to the drier winter in the Australian monsoon
246 region, but the local dynamic processes play a dominant role in the reduction of Australian
247 winter precipitation.

248 3.2 Why the precipitation increased in austral early summer (ND)

249 During ND, the LGM minus PI surface wind difference field shows a strengthened
250 convergence pattern over the central northern Australian monsoon region (Fig. 6a, vector), which
251 is consistent with the increased precipitation (Fig. 6a, shading). The vertical velocity at 500 hPa
252 also shows a strengthened ascending flow over this area (Fig. 7). The increased precipitation
253 over the central Australian monsoon region is clearly against the thermodynamic effects of the
254 low GHG concentration and the presence of the ice-sheets, which tends to reduce the
255 precipitation. The 2-m air temperature was decreased by 2.2 K and the surface specific humidity
256 reduced by 2.6 g/kg (or 16.0 %) over the Australian monsoon region (Fig. 8). The precipitation

257 would decrease by 15.4 % according to the thermal effect without the circulation change.
258 However, the precipitation over the Australian monsoon region increased by about 13.0 %.
259 Therefore, the changes in dynamic processes must induce a 29 % increase of precipitation, so
260 that the net increase in precipitation reaches 13 %.

261 There is a cyclonic wind anomaly associated with an anomalous low pressure over the
262 northwest Australia (Fig. 6a and Fig. 9b, vector), accompanied by a strengthened low-level
263 convergence (Fig. 9c), which favors increased precipitation in the Australian monsoon region.
264 The change of the moisture transport (moisture flux) also indicated increased moisture transport
265 into northern Australia (not shown). The cyclonic vorticity in northwest Australia is partially
266 caused by the enhanced strong low-level westerlies that prevail north of Australia.

267 We now seek to determine why there was a strengthened low-level westerly with
268 maximum over north of Australia. We first consider the temperature change. The ND mean 2-m
269 air temperature during the LGM shows that the two enlarged landmasses over the Indo-Pacific
270 warm pool region (resulting from the lower sea level) change differently (Fig. 9a). It is cooler
271 over the northwest landmass (western Indonesia–Indochina) and relatively warmer over the
272 southeast landmass (eastern Indonesia–northern Australia). This temperature variation forms a
273 southeast–northwest temperature gradient (Fig. 9a, Fig. S5a, S5b), accompanied by a northwest–
274 southeast SLP gradient (Fig. 9b, Fig. S5c, S5d). The northwest–southeast pressure gradient is
275 stronger in the geopotential height change at 850 hPa (Fig. S4b). The high pressure in the
276 western Indonesia–Indochina is a part of the larger scale enhanced winter monsoon over the
277 South China Sea. This enhanced winter monsoon flows cross the equator from the NH to the SH
278 and turn into strong westerlies due to deflection induced by the Coriolis force. The 850 hPa
279 convergence strengthens over the Australian monsoon region (Fig. 9c), and the corresponding
280 ascending motion at 500 hPa also increases over the Australian monsoon region.

281 Another reason for circulation change is the sea surface temperature (SST) gradient
282 change. The SST anomaly in ND shows a warmer Western Pacific and cooler Eastern Indian
283 Ocean pattern (Fig. 10), indicating a westward temperature gradient (Fig. S5e), and thus an
284 eastward pressure gradient which, in the equatorial region, can directly enhance westerly winds
285 near the northern Australian monsoon region (Fig. 9b). Li et al. (2012) also found that a cold
286 state of the Wharton Basin (100°E–130°E, 20°S–5°S) was accompanied by anomalous westerlies

287 and cyclonic circulation anomalies in the Australian monsoon region, which were associated
288 with a strong tropical Australian summer monsoon and enhanced rainfall over northeast
289 Australia.

290 In summary, during ND, the enlarged land area due to sea-level drop enhances the land–
291 sea thermal contrast, and forms a northwest–southeast thermal contrast which induces low
292 pressure over northern Australia but high pressure over the adjacent ocean and the Indochina–
293 western Indonesia, leading to enhanced convergence over northern Australia and thus increasing
294 the early summer monsoon rainfall. The SST gradients between the warm equatorial western
295 Pacific and relatively cool eastern Indian Ocean during the pre-summer monsoon season also
296 contribute to the strengthened equatorial westerlies and the cyclonic wind anomaly over northern
297 Australia. These dynamic mechanisms have a positive contribution to the early summer
298 precipitation. The thermal effects have negative contribution to the precipitation change, but with
299 smaller impact. Therefore, the early summer precipitation over northern Australia increases. We
300 can also tell from the changes of the decomposed terms that the dynamics plays much more
301 important role in the precipitation change over Australia, especially the distribution pattern (Fig.
302 S6). Again, the impacts of evaporation and advection terms are small.

303

304 **4 Discussion**

305 The intensification of the Australian monsoon in this study is measured by the enhanced
306 seasonal difference (or the seasonality) of precipitation, and is particularly attributed to the
307 decreased austral winter precipitation. This is consistent with the reconstructed results by
308 Mohtadi et al. (2011), which indicated that it was not significantly drier in austral summer during
309 the LGM, while (the winter monsoon is weakened). Whereas the annual mean precipitation is
310 decreased, which means the Australian monsoon would be weakened during the LGM when it is
311 measured by the annual mean precipitation. The modeling study by DiNezio et al. (2013)
312 suggests a decreasing rainfall across northern Australia during the LGM, consistent with the
313 proxy synthesis by stalagmite (Denniston et al., 2017). The decreased rainfall in their work
314 represents the annual mean precipitation, which also consists with our work in this point of view.
315 On the other hand, the increased rainfall in austral summer in this study is consistent with what
316 has been revealed in the reconstructed work by Liu et al. (2015). The decreased annual mean

317 precipitation and the intensified seasonality of precipitation over the Australian monsoon region
318 are in agreement with the synthesis from the simulated result by Tharammal et al. (2013) using a
319 set of experiments.

320 For the forcings and mechanisms of the Australian monsoon change during the LGM,
321 there are large changes in four external forcings during the LGM, including the insolation change
322 resulting from the orbital change, the land–sea configuration change, the GHG change and the
323 presence of ice-sheets. The lower GHG concentrations and the presence of ice-sheets are likely
324 to be contributors to the thermal effect leading to the reduced water vapor and thus the decreased
325 rainfall both in austral winter and early summer. The enlarged the landmasses over western
326 Indonesia and northeastern Australia are essential to the local dynamic processes that influence
327 the rainfall. The low obliquity and high precession during the LGM may be another factor that
328 can affect the rainfall (Liu et al., 2015). However, the impact of the insolation change caused by
329 the orbital change remains unknown.

330 During the LGM, the insolation over tropical region increased from December to June
331 and decreased from July to November (Fig. 11a). In the annual variation, precipitation responds
332 to the lower tropospheric moisture convergence. The moisture change depends on temperature
333 change while the circulation change depends on surface temperature gradients change. The
334 change of the surface temperature lags insolation changes because of the ocean and land surfaces
335 have heat capacity (thermal inertial). In other words, insolation is a heating rate which equals to
336 temperature change (tendency) but not the temperature itself. Thus the precipitation change
337 would lag the insolation change by about two months, due to the ocean–atmosphere interaction
338 without other processes. For example, the change of seasonal distribution of NH monsoon
339 precipitation lagged the change of the NH insolation by one month (Yan et al., 2016). Whereas
340 in this study, the Australian monsoon precipitation decreased from March to September and
341 increased from November to February (Fig. 11b), quite different from what it would be (i.e.,
342 decrease from September to January and increase from February to August). Meanwhile, the
343 insolation over SH increased during the LGM from April to August, when Australia is in late
344 autumn and winter. An increased insolation might make land warmer than ocean thus against the
345 climatology, which may be described by cooler land and warmer ocean in winter. However, the
346 simulated surface temperature reduced more over Australia than the adjacent oceans (Fig. 5a).
347 On the other hand, the synthesis of Wyrwoll et al. (2007) and Liu et al. (2015) indicates the

348 strong convergence rain belt (ITCZ) stays in the north, resulting in more rainfall over Papua New
349 Guinea and less rainfall over North Australia during those times with low obliquity and high
350 precession. The rain belt stays a little more northerly than that stays in our study, which means
351 the effect of orbital change and thus the insolation change might be suppressed by other factors.

352 Moreover, the paleoclimate records suggest that it was dry and cool in the Indo-Pacific
353 Warm Pool region during the LGM (Xu et al., 2010). The simulated SST is consistent with the
354 reconstructions. Although in the early austral summer, over the Indian Ocean warm pool, it is
355 cooler over the SH, while over the Pacific warm pool, it is cooler over the NH (Fig. S7). Such
356 anomalous SST asymmetry may favor the southward shift of the ITCZ over Australia and the
357 southwest Pacific, which might be related to the enhanced austral summer monsoon
358 precipitation. However, the 7MME shows no significant ITCZ shift during the LGM, particularly
359 over the central Australian monsoon region (Fig. S8). The reconstructions and simulations by
360 McGee et al. (2014) and Mohtadi et al. (2014) also suggested that there was no significant shift
361 of ITCZ position during the LGM.

362 Therefore, it is the local dynamical processes, instead of the large-scale circulation such
363 as the position of the ITCZ induced by the NH-SH thermal contrast, that might be the key factor
364 influencing the early summer mean precipitation change over the Australian monsoon region
365 during the LGM. To test this synthesis, we conducted two experiments using a newly developed
366 earth system model, the Nanjing University of Information Science and Technology Earth
367 System model version 1 (NESM v1, Cao et al., 2015). The PI control run is designed the same as
368 PMIP3 protocol. The land sea configuration sensitive run (LSM) is the same as the piControl but
369 with the LGM land sea configuration. The two experiments are run 500 years after spin-up, and
370 the last 100 years are used. The changes of the ND mean precipitation and wind field at 1000
371 hPa between LSM and piControl are similar to the changes derived from the 7MME, i.e. the
372 precipitation is increased and the convergence is strengthened over northern Australia (Fig. 12a).
373 The changes of the 2-m air temperature, SLP and 850 hPa wind field (Fig. 12b, c) are also
374 similar to those results in the 7MME (Fig. 9). It is also cooler over the northwest landmass
375 (western Indonesia–Indochina) and relatively warmer over the southeast landmass (eastern
376 Indonesia–northern Australia) (Fig. 12b). This temperature variation is also accompanied by a
377 northwest–southeast SLP gradient and the strengthened cross equatorial flow converging to north

378 Australia (Fig. 12c). This sensitive simulation confirms that the local dynamical process induced
379 by the land sea configuration to be essential to the Australian monsoonality change.

380 Although the 7MME simulates strengthened Australian monsoonality, there are
381 uncertainties among individual models. The most notable uncertainty is the increased austral
382 summer (DJF) precipitation. Five out of the 7 models simulate increased DJF mean precipitation
383 over the Australian monsoon region during the LGM (CCSM4, GISS-E2-R, IPSL-CM5A-LR,
384 MIROC-ESM and MRI-CGCM3), while the other two simulate decreased precipitation (CNRM-
385 CM5 and MPI-ESM-P) (Fig. 13), especially over the land area. The wind field at 850hPa
386 geopotential height shows a cyclonic anomaly pattern over northern Australia in the five models
387 (Fig. 14a), accompanied with a strengthened ascending flow (not shown). While in the other two
388 models, there is no cyclonic wind anomaly over Australia region (Fig. 14b), and the ascending
389 flow is weakened (not shown). The different changes of wind field indicate the different
390 precipitation responses to the LGM boundary conditions in the two model groups.

391 The austral spring and summer mean 2m-air temperature and SST also change differently
392 in these two model groups. The main differences are located over the tropic Pacific Ocean and
393 the North Atlantic Ocean. It is cooler over high-latitude Northern Atlantic Ocean in the five
394 models, whereas warmer in the two models, mainly in the austral spring (Fig. 15a, 15b). In the
395 austral summer, there is an East-Pacific El Nino like pattern in the five models, while there is a
396 Central-Pacific El Nino (CP-El Nino) like pattern in the two models (Fig. 15c, 15d). Studies have
397 shown that the CP-El Nino is related to the Asian-Australian monsoon system (Yu et al. 2009),
398 and would lead to a markedly decreased precipitation in December (Taschetto et al. 2009).

399 Therefore, the different SST response over Pacific Oceans and North Atlantic Ocean in
400 austral spring and summer in different models might be the key factor that leads to different wind
401 anomalies and thus different Australian monsoon precipitation changes.

402

403 **5 Conclusions**

404 The global mean temperature and water vapor have an overall decrease under the LGM
405 forcings (lower GHG and large ice-sheets). Nevertheless, the simulated Australian monsoon
406 seasonality derived from CMIP5/PMIP3 multi-model ensemble has a distinctive amplification
407 (or the monsoonality is intensified) against the weakened global monsoons elsewhere during the

408 LGM. This study then investigated the possible reasons for this strengthened Australian
409 monsoonality from both a thermodynamic and dynamic perspective.

410 The conclusions are as follows:

- 411 1) The Australian monsoon seasonality is strengthened as a result of the enhanced
412 seasonal difference between austral summer and winter, i.e., the increased early
413 summer (ND) mean rainfall and the reduced winter (JJA) mean rainfall. Both the
414 dynamic processes and thermal effects contribute to the precipitation change; however,
415 the dynamic processes have a much stronger contribution than the thermal effects.
- 416 2) The Australian winter (JJA mean) precipitation derived from 7MME decreased during
417 the LGM relative to the preindustrial control experiment. The dynamic processes,
418 induced by the enhanced land–ocean thermal contrast, contribute more to the decreased
419 rainfall through the strengthened divergence over northern Australia (Fig. 16a),
420 whereas the thermodynamic effect (i.e., the reduced atmospheric water vapor due to the
421 lower temperature induced by lower GHGs and present ice-sheets) and evaporation
422 have moderate contribution.
- 423 3) For the increased precipitation in early summer (ND) in the 7MME, the local dynamic
424 processes have a positive contribution and the thermodynamic effect has a negative
425 contribution. Both the decomposition method and the sensitive simulations show that
426 the dynamic effect plays most important role for the increased rainfall. The local
427 dynamic processes are mainly induced by the northwest–southeast thermal contrast
428 between Indochina–western Indonesia and northeastern Australia. The east Indian
429 Ocean–west Pacific Ocean thermal gradient also contributes to these processes (Fig.
430 16b).
- 431 4) The sensitive simulation illustrates that the change in circulation over Australia is very
432 likely to be rooted in the enlarged landmasses over the Indochina–western Indonesia
433 and New Guinea, and northern Australia. Another factor contributes to the circulation
434 change might be the asymmetric change between western Pacific Ocean and eastern
435 Indian Ocean. These have critical impacts on the thermal gradients that induce changes
436 in the low-level circulation pattern and convergence/divergence.

437 Note that models have uncertainties, i.e. not all the models simulate an intensified
438 seasonality of Australian monsoon. The different SST responses over Pacific Ocean and Atlantic
439 Ocean in different models to the same external forcings are essential for the model uncertainties.
440 More model-data comparison and inter-model comparison are required to improve model
441 performance.

442 Our results are based on the equilibrium simulation, representing a mean state of the
443 Australian monsoon change and its possible mechanisms during the LGM. More simulations
444 with single forcing (such as the SST asymmetry change, the insolation change) are required to
445 further understand the effect of each factor and to specifically quantify the contribution of each
446 forcing to the Australian monsoon change.

447

448 **Acknowledgments**

449 We acknowledge Prof. Williams J and the two reviewers for the comments helping to
450 clarify and improve the paper. This research was jointly supported by the National Key Research
451 and Development Program of China (Grant No. 2016YFA0600401), the National Basic Research
452 Program (Grant No. 2015CB953804), the National Natural Science Foundation of China (Grant
453 Nos. 41671197, 41420104002 and 41501210), and the Priority Academic Development Program
454 of Jiangsu Higher Education Institutions (PAPD, Grant No. 164320H116). We acknowledge the
455 World Climate Research Programme’s Working Group on Coupled Modeling, which is
456 responsible for the CMIP, and we thank the climate modeling groups for producing and making
457 available their model outputs. For the CMIP, the U.S. Department of Energy’s Program for
458 climate model diagnosis and intercomparison provided coordinating support and led the
459 development of software infrastructure in partnership with the Global Organization for Earth
460 System Science Portals. We thank LetPub (www.letpub.com) for its linguistic assistance during
461 the preparation of this manuscript. This is the ESMC publication XXX.

462

463 **References**

- 464 Ayliffe, L. K., Gagan, M. K., Zhao, J. X., Drysdale, R. N., Hellstrom, J. C., Hantoro, W. S.,
465 Griffiths, M. L., Scott-Gagan, H., St Pierre, E., Cowley, J. A., and Suwargadi, B. W.: Rapid
466 interhemispheric climate links via the Australasian monsoon during the last deglaciation,
467 *Nat Commun*, 4, 2908, 10.1038/ncomms3908, 2013.
- 468 Bayon, G., De Deckker, P., Magee, J. W., Germain, Y., Bermell, S., Tachikawa, K., and
469 Norman, M. D.: Extensive wet episodes in Late Glacial Australia resulting from high-
470 latitude forcings, *Scientific Reports*, 7, 44054, 10.1038/srep44054, 2017.
- 471 Braconnot, P., Otto-Bliesner, B., Harrison, S. P., and al, e.: Results of PMIP2 coupled
472 simulations of the Mid-Holocene and Last Glacial Maximum – Part 2: feedbacks with
473 emphasis on the location of the ITCZ and mid- and high latitudes heat budget, *Climate of*
474 *the Past*, 3, 2007.
- 475 Braconnot, P., Harrison, S. P., Kageyama, M., Bartlein, P. J., Masson-Delmotte, V., Abe-Ouchi,
476 A., Otto-Bliesner, B., and Zhao, Y.: Evaluation of climate models using palaeoclimatic data,
477 *Nature Climate Change*, 2, 417-424, 10.1038/nclimate1456, 2012a.
- 478 Braconnot, P., Harrison, S. P., Otto-Bliesner, B., Abe-Ouchi, A., Jungclauss, J., and Peterschmitt,
479 J. Y.: The Paleoclimate Modeling Intercomparison Project contribution to CMIP5, *CLIVAR*
480 *Exchanges*, 56, 15-19, 2012b.
- 481 Broccoli, A. J., Dahl, K. A., and Stouffer, R. J.: Response of the ITCZ to Northern Hemisphere
482 cooling, *Geophysical Research Letters*, 33(1), L01702, 10.1029/2005gl024546, 2006.
- 483 Brown, J. R., Moise, A. F., Colman, R., and Zhang, H.: Will a Warmer World Mean a Wetter or
484 Drier Australian Monsoon? *Journal of Climate*, 29, 4577-4596, 10.1175/jcli-d-15-0695.1,
485 2016.
- 486 Cao, J., Wang, B., Xiang, B., Li, J., Wu, T., Fu, X., Wu, L., and Min, J.: Major modes of short-
487 term climate variability in the newly developed NUIST Earth System Model (NESM),
488 *Advances in Atmospheric Sciences*, 32, 585-600, 10.1007/s00376-014-4200-6, 2015.
- 489 Chou, C., Neelin, J. D., Chen, C.-A., and Tu, J.-Y.: Evaluating the “Rich-Get-Richer”
490 Mechanism in Tropical Precipitation Change under Global Warming, *Journal of Climate*,
491 22, 1982-2005, 10.1175/2008jcli2471.1, 2009.

492 Cui, X. P.: Quantitative diagnostic analysis of surface rainfall processes by surface rainfall
493 equation. *Chinese Journal of Atmospheric Sciences*, 33(2), 375–387, 2009.

494 De Deckker, P., Barrows, T. T., and Rogers, J.: Land–sea correlations in the Australian region:
495 post-glacial onset of the monsoon in northwestern Western Australia, *Quaternary Science*
496 *Reviews*, 105, 181-194, 10.1016/j.quascirev.2014.09.030, 2014.

497 Denniston, R. F., Wyrwoll, K.-H., Asmerom, Y., Polyak, V. J., Humphreys, W. F., Cugley, J.,
498 Woods, D., LaPointe, Z., Peota, J., and Greaves, E.: North Atlantic forcing of millennial-
499 scale Indo-Australian monsoon dynamics during the Last Glacial period, *Quaternary*
500 *Science Reviews*, 72, 159-168, 10.1016/j.quascirev.2013.04.012, 2013.

501 Denniston, R. F., Asmerom, Y., Polyak, V. J., Wanamaker, A. D., Ummenhofer, C. C.,
502 Humphreys, W. F., Cugley, J., Woods, D., and Lucker, S.: Decoupling of monsoon activity
503 across the northern and southern Indo-Pacific during the Late Glacial, *Quaternary Science*
504 *Reviews*, 176, 101-105, 10.1016/j.quascirev.2017.09.014, 2017.

505 DiNezio, P. N., Timmermann, A., Tierney, J. E., Jin, F.-F., Otto-Bliesner, B., Rosenbloom, N.,
506 Mapes, B., Neale, R., Ivanovic, R. F., and Montenegro, A.: The climate response of the
507 Indo-Pacific warm pool to glacial sea level, *Paleoceanography*, 31, 866-894,
508 10.1002/2015PA002890, 2016.

509 DiNezio, P. N., Clement, A., Vecchi, G. A., Soden, B., Broccoli, A. J., Otto-Bliesner, B. L., and
510 Braconnot, P.: The response of the Walker circulation to Last Glacial Maximum forcing:
511 Implications for detection in proxies, *Paleoceanography*, 26, n/a-n/a,
512 10.1029/2010pa002083, 2011.

513 DiNezio, P. N., and Tierney, J. E.: The effect of sea level on glacial Indo-Pacific climate, *Nature*
514 *Geoscience*, 6, 485-491, 10.1038/ngeo1823, 2013.

515 Donohoe, A., Marshall, J., Ferreira, D., and McGee, D.: The Relationship between ITCZ
516 Location and Cross-Equatorial Atmospheric Heat Transport: From the Seasonal Cycle to
517 the Last Glacial Maximum, *Journal of Climate*, 26, 3597-3618, 10.1175/jcli-d-12-00467.1,
518 2013.

519 Endo, H., and Kitoh, A.: Thermodynamic and dynamic effects on regional monsoon rainfall
520 changes in a warmer climate, *Geophysical Research Letters*, 41, 1704-1711,
521 10.1002/2013gl059158, 2014.

522 Eroglu, D., McRobie, F. H., Ozken, I., Stemler, T., Wyrwoll, K. H., Breitenbach, S. F., Marwan,
523 N., and Kurths, J.: See-saw relationship of the Holocene East Asian-Australian summer
524 monsoon, *Nat Commun*, 7, 12929, 10.1038/ncomms12929, 2016.

525 Hargreaves, J. C., Annan, J. D., Ohgaito, R., Paul, A., and Abe-Ouchi, A.: Skill and reliability of
526 climate model ensembles at the Last Glacial Maximum and mid-Holocene, *Climate of the*
527 *Past*, 9, 811-823, 10.5194/cp-9-811-2013, 2013.

528 Harrison, S. P., Bartlein, P. J., Brewer, S., Prentice, I. C., Boyd, M., Hessler, I., Holmgren, K.,
529 Izumi, K., and Willis, K.: Climate model benchmarking with glacial and mid-Holocene
530 climates, *Climate Dynamics*, 43, 671-688, 10.1007/s00382-013-1922-6, 2014.

531 Held, I. M., and Soden, B. J.: Robust responses of the hydrological cycle to global warming,
532 *Journal of Climate*, 19, 5686-5699, 2006.

533 Hewitt, C., Broccoli, A. J., Mitchell, J. F. B., and Stouffer, R.: A coupled model study of the last
534 glacial maximum: Was part of the North Atlantic relatively warm? *Geophys. Res. Lett.*, 28,
535 1571-1574, 2001.

536 Huang, P., Xie, S.-P., Hu, K., Huang, G., and Huang, R.: Patterns of the seasonal response of
537 tropical rainfall to global warming, *Nature Geoscience*, 6, 357-361, 10.1038/ngeo1792,
538 2013.

539 Huffman, G. J., Adler, R. F., Bolvin, D. T., and Gu, G.: Improving the global precipitation
540 record: GPCP Version 2.1, *Geophysical Research Letters*, 36, 10.1029/2009gl040000, 2009.

541 Jiang, D., Tian, Z., Lang, X., Kageyama, M., and Ramstein, G.: The concept of global monsoon
542 applied to the last glacial maximum: A multi-model analysis, *Quaternary Science Reviews*,
543 126, 126-139, 10.1016/j.quascirev.2015.08.033, 2015.

544 Jourdain, N. C., Gupta, A. S., Taschetto, A. S., Ummenhofer, C. C., Moise, A. F., and Ashok, K.:
545 The Indo-Australian monsoon and its relationship to ENSO and IOD in reanalysis data and
546 the CMIP3/CMIP5 simulations, *Climate Dynamics*, 41, 3073-3102, 10.1007/s00382-013-
547 1676-1, 2013.

548 Kuhnt, W., Holbourn, A., Xu, J., Opdyke, B., De Deckker, P., Rohl, U., and Mudelsee, M.:
549 Southern Hemisphere control on Australian monsoon variability during the late deglaciation
550 and Holocene, *Nat Commun*, 6, 5916, 10.1038/ncomms6916, 2015.

551 Li, J., Feng, J., and Li, Y.: A possible cause of decreasing summer rainfall in northeast Australia,
552 *International Journal of Climatology*, 32, 995-1005, 10.1002/joc.2328, 2012.

553 Liu, F., Chai, J., Wang, B., Liu, J., Zhang, X., and Wang, Z.: Global monsoon precipitation
554 responses to large volcanic eruptions, *Sci Rep*, 6, 24331, 10.1038/srep24331, 2016.

555 Liu, Y., Lo, L., Shi, Z., Wei, K. Y., Chou, C. J., Chen, Y. C., Chuang, C. K., Wu, C. C., Mii, H.
556 S., Peng, Z., Amakawa, H., Burr, G. S., Lee, S. Y., DeLong, K. L., Elderfield, H., and Shen,
557 C. C.: Obliquity pacing of the western Pacific Intertropical Convergence Zone over the past
558 282,000 years, *Nat Commun*, 6, 10018, 10.1038/ncomms10018, 2015.

559 Marshall, A. G., and Lynch, A. H.: Time-slice analysis of the Australian summer monsoon
560 during the late Quaternary using the Fast Ocean Atmosphere Model, *Journal of Quaternary*
561 *Science*, 21, 789-801, 10.1002/jqs.1063, 2006.

562 Marshall, A. G., and Lynch, A. H.: The sensitivity of the Australian summer monsoon to climate
563 forcing during the late Quaternary, *Journal of Geophysical Research*, 113,
564 10.1029/2007jd008981, 2008.

565 McGee, D., Donohoe, A., Marshall, J., and Ferreira, D.: Changes in ITCZ location and cross-
566 equatorial heat transport at the Last Glacial Maximum, Heinrich Stadial 1, and the mid-
567 Holocene, *Earth and Planetary Science Letters*, 390, 69-79, 10.1016/j.epsl.2013.12.043,
568 2014.

569 Miller, G. H., Fogel, M. L., Magee, J. W., and Gagan, M. K.: Disentangling the impacts of
570 climate and human colonization on the flora and fauna of the Australian arid zone over the
571 past 100 ka using stable isotopes in avian eggshell, *Quaternary Science Reviews*, 151, 27-
572 57, 10.1016/j.quascirev.2016.08.009, 2016.

573 Mohtadi, M., Prange, M., Oppo, D. W., De Pol-Holz, R., Merkel, U., Zhang, X., Steinke, S., and
574 Lückge, A.: North Atlantic forcing of tropical Indian Ocean climate, *Nature*, 509, 76,
575 10.1038/nature13196, 2014.

576 Petherick, L., Bostock, H., Cohen, T. J., Fitzsimmons, K., Tibby, J., Fletcher, M. S., Moss, P.,
577 Reeves, J., Mooney, S., Barrows, T., Kemp, J., Jansen, J., Nanson, G., and Dosseto, A.:
578 Climatic records over the past 30 ka from temperate Australia – a synthesis from the Oz-
579 INTIMATE workgroup, *Quaternary Science Reviews*, 74, 58-77,
580 10.1016/j.quascirev.2012.12.012, 2013.

581 Reeves, J. M., Barrows, T. T., Cohen, T. J., Kiem, A. S., Bostock, H. C., Fitzsimmons, K. E.,
582 Jansen, J. D., Kemp, J., Krause, C., Petherick, L., and Phipps, S. J.: Climate variability over
583 the last 35,000 years recorded in marine and terrestrial archives in the Australian region: an
584 OZ-INTIMATE compilation, *Quaternary Science Reviews*, 74, 21-34,
585 10.1016/j.quascirev.2013.01.001, 2013a.

586 Reeves, J. M., Bostock, H. C., Ayliffe, L. K., Barrows, T. T., De Deckker, P., Devriendt, L. S.,
587 Dunbar, G. B., Drysdale, R. N., Fitzsimmons, K. E., Gagan, M. K., Griffiths, M. L.,
588 Haberle, S. G., Jansen, J. D., Krause, C., Lewis, S., McGregor, H. V., Mooney, S. D., Moss,
589 P., Nanson, G. C., Purcell, A., and van der Kaars, S.: Palaeoenvironmental change in
590 tropical Australasia over the last 30,000 years – a synthesis by the OZ-INTIMATE group,
591 *Quaternary Science Reviews*, 74, 97-114, 10.1016/j.quascirev.2012.11.027, 2013b.

592 Rojas, M.: Sensitivity of Southern Hemisphere circulation to LGM and $4 \times \text{CO}_2$ climates,
593 *Geophysical Research Letters*, 40, 965-970, 10.1002/grl.50195, 2013.

594 Seager, R., Naik, N., and Vecchi, G. A.: Thermodynamic and Dynamic Mechanisms for Large-
595 Scale Changes in the Hydrological Cycle in Response to Global Warming*, *Journal of*
596 *Climate*, 23, 4651-4668, 10.1175/2010jcli3655.1, 2010.

597 Taylor, K. E., Stouffer, R. J., and Meehl, G. A.: An Overview of CMIP5 and the Experiment
598 Design, *Bulletin of the American Meteorological Society*, 93, 485-498, 10.1175/bams-d-11-
599 00094.1, 2012.

600 Tharammal, T., Paul, A., Merkel, U., and Noone, D.: Influence of Last Glacial Maximum
601 boundary conditions on the global water isotope distribution in an atmospheric general
602 circulation model, *Climate of the Past*, 9, 789-809, 10.5194/cp-9-789-2013, 2013.

603 Turney, C. S. M., Haberle, S., Fink, D., Kershaw, A. P., Barbetti, M., Barrows, T. T., Black, M.,
604 Cohen, T. J., Corrège, T., Hesse, P. P., Hua, Q., Johnston, R., Morgan, V., Moss, P.,

605 Nanson, G., van Ommen, T., Rule, S., Williams, N. J., Zhao, J. X., D'Costa, D., Feng, Y.
606 X., Gagan, M., Mooney, S., and Xia, Q.: Integration of ice-core, marine and terrestrial
607 records for the Australian Last Glacial Maximum and Termination: a contribution from the
608 OZ INTIMATE group, *Journal of Quaternary Science*, 21, 751-761, 10.1002/jqs.1073,
609 2006.

610 Wang, B., and Ding, Q.: Global monsoon: Dominant mode of annual variation in the tropics,
611 *Dynamics of Atmospheres and Oceans*, 44, 165-183, 10.1016/j.dynatmoce.2007.05.002,
612 2008.

613 Wang, P. X., Wang, B., Cheng, H., Fasullo, J., Guo, Z., Kiefer, T., and Liu, Z.: The global
614 monsoon across time scales: Mechanisms and outstanding issues, *Earth-Science Reviews*,
615 10.1016/j.earscirev.2017.07.006, 2017.

616 Williams, A. N., Ulm, S., Cook, A. R., Langley, M. C., and Collard, M.: Human refugia in
617 Australia during the Last Glacial Maximum and Terminal Pleistocene: a geospatial analysis
618 of the 25–12 ka Australian archaeological record, *Journal of Archaeological Science*, 40,
619 4612-4625, 10.1016/j.jas.2013.06.015, 2013.

620 Wyrwoll, K.-H., Liu, Z., Chen, G., Kutzbach, J. E., and Liu, X.: Sensitivity of the Australian
621 summer monsoon to tilt and precession forcing, *Quaternary Science Reviews*, 26, 3043-
622 3057, 10.1016/j.quascirev.2007.06.026, 2007.

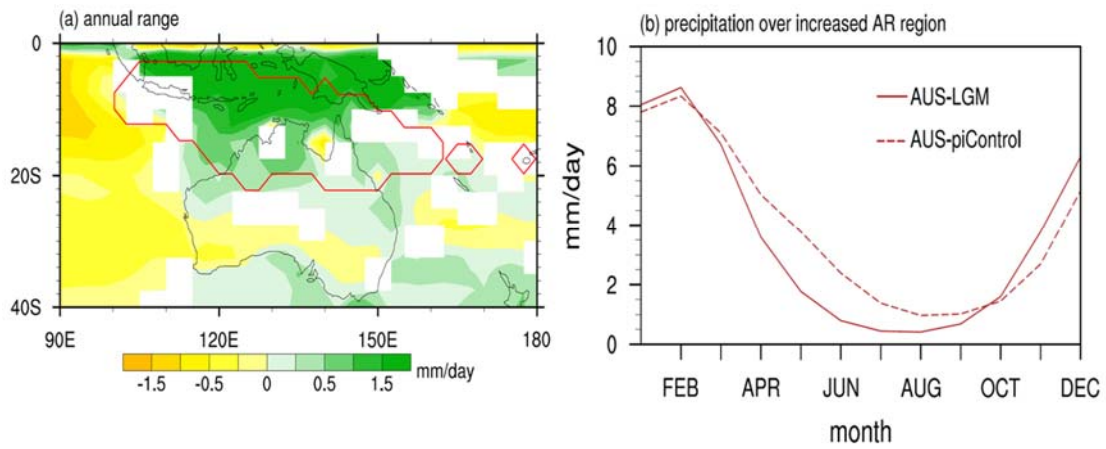
623 Wyrwoll, K.-H., Hopwood, J. M., and Chen, G.: Orbital time-scale circulation controls of the
624 Australian summer monsoon: a possible role for mid-latitude Southern Hemisphere forcing?
625 *Quaternary Science Reviews*, 35, 23-28, 10.1016/j.quascirev.2012.01.003, 2012.

626 Xie, P., and Arkin, P.: Global precipitation: a 17-year monthly analysis based on Gauge
627 Observations, satellite estimates, and numerical model outputs, *Bulletin of the American*
628 *Meteorological Society*, 78, 2539-2558, 1997.

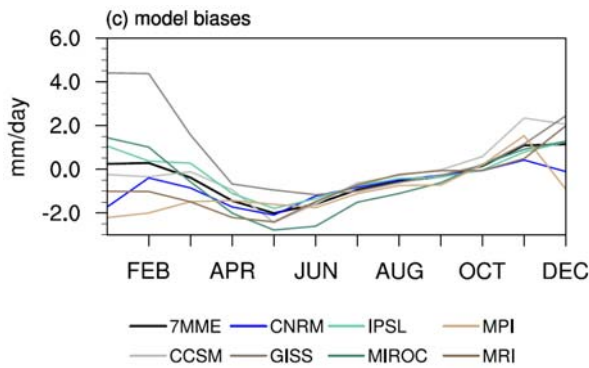
629 Xu, J., Kuhnt, W., Holbourn, A., Regenberg, M., and Andersen, N.: Indo-Pacific Warm Pool
630 variability during the Holocene and Last Glacial Maximum, *Paleoceanography*, 25,
631 10.1029/2010pa001934, 2010.

632 Yan, M., Wang, B., and Liu, J.: Global monsoon change during the Last Glacial Maximum: a
633 multi-model study, *Climate Dynamics*, 47, 359-374, 10.1007/s00382-015-2841-5, 2016.

635



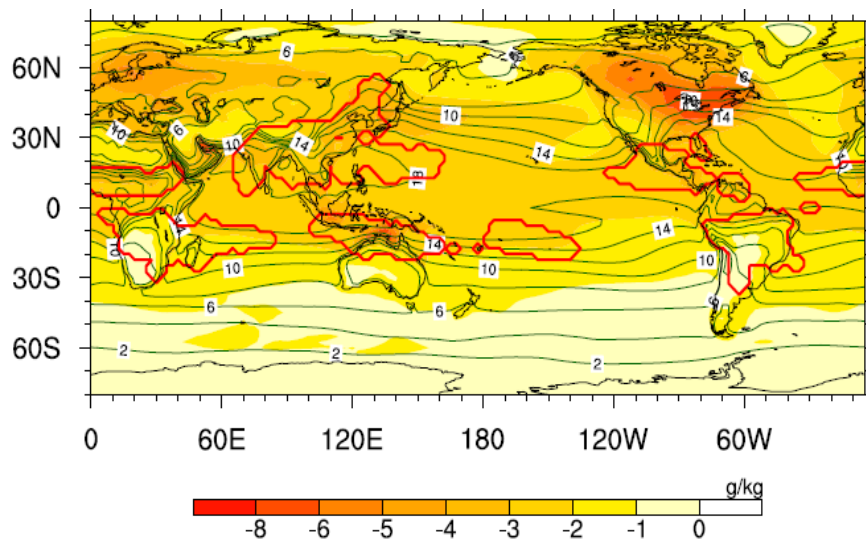
636



637

638 **Figure 1** (a) Spatial distribution of changes in the annual range (AR) of precipitation measured
639 by the difference between LGME and piControl, (b) seasonal distribution of the precipitation in
640 the increased AR area (20°S-5°S, 120°E-145°E), and (c) seasonal distribution of the precipitation
641 differences in the increased AR area derived from 7 MME (black line) and each model (colored
642 lines). The red solid line in (a) encloses the Australian monsoon rainfall domain. The dashed
643 (solid) line in (b) denotes the seasonal distribution of precipitation derived from the piControl
644 (LGME) run. Only those areas where signal-to-noise ratio exceeds one are plotted in (a).

645

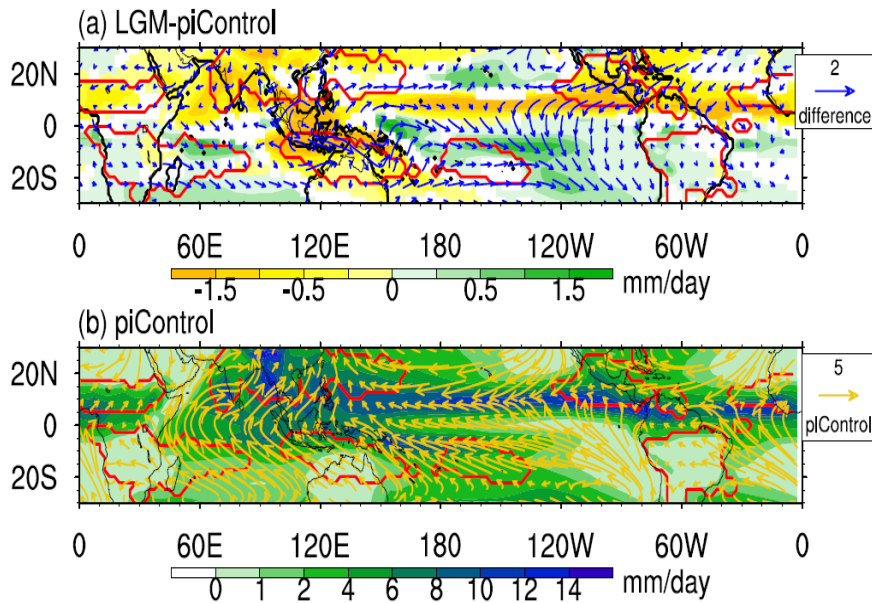


646

647 **Figure 2** Difference of JJA mean surface specific humidity between LGME and piControl
 648 (shaded). The green contours denote the climatology derived from piControl. The red lines
 649 enclose the monsoon domains. Only those areas where signal-to-noise ratio exceeds one are
 650 plotted.

651

652

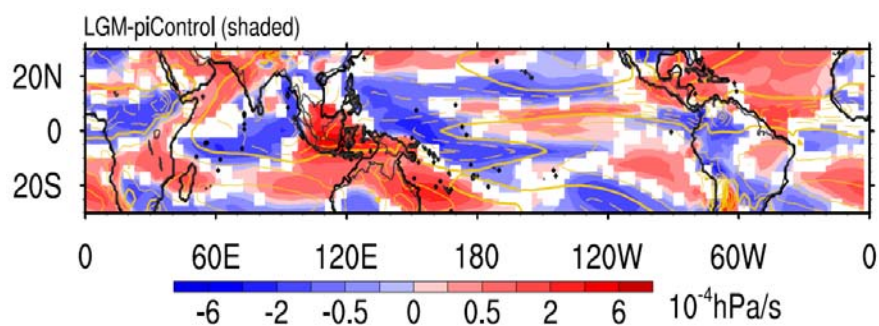


653

654 **Figure 3** (a) JJA mean precipitation (shading) difference and surface wind (vectors) difference
655 between LGME and piControl, and (b) the climatology of JJA mean precipitation (shading) and
656 surface wind (vectors) derived from piControl. The red lines enclose the monsoon domains. The
657 thick black lines in (a) denote the coastal lines in LGME, and the thin black lines denote the
658 coastal lines in piControl. Only those areas where signal-to-noise ratio exceeds one are plotted in
659 (a).

660

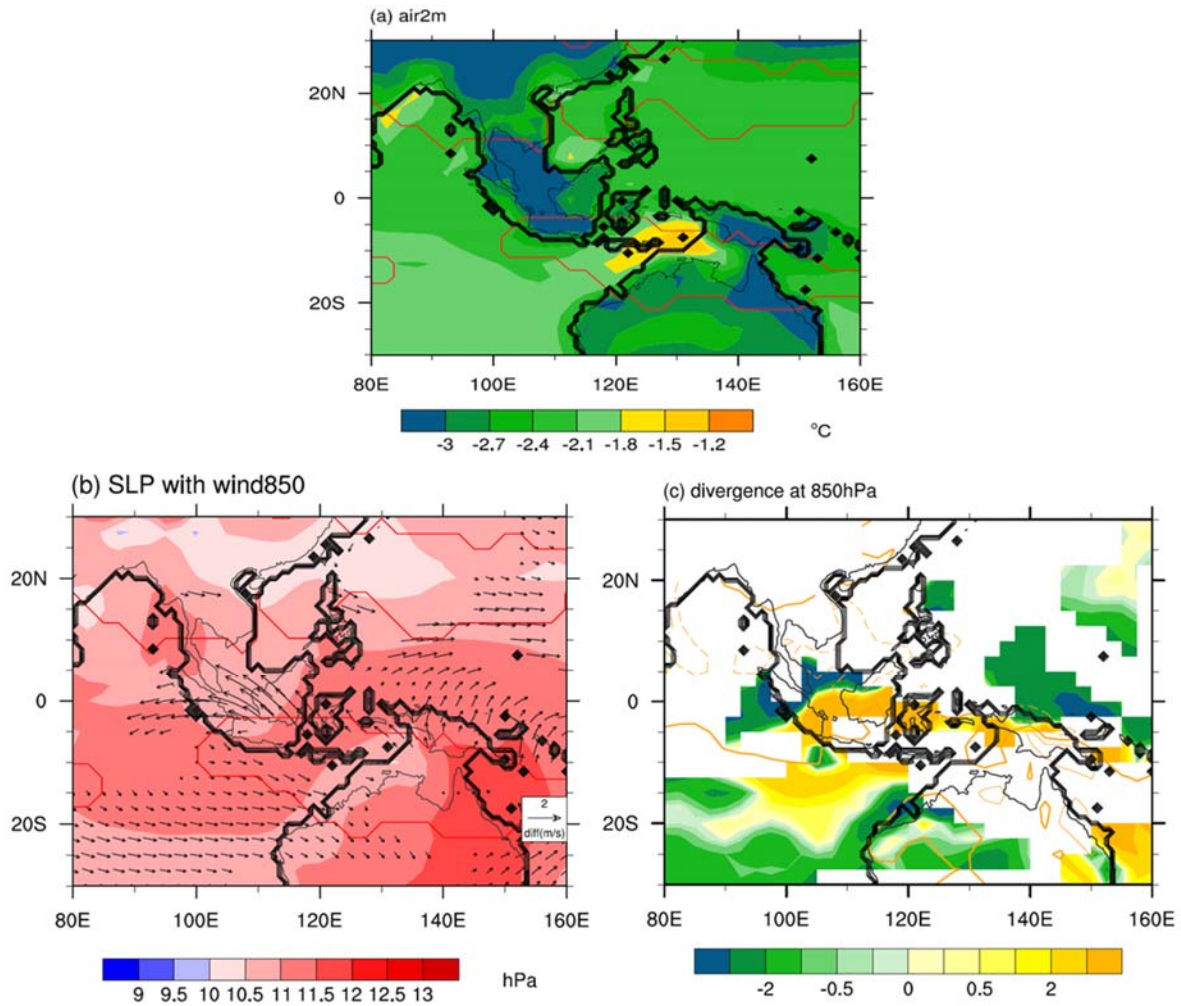
661



662

663 **Figure 4** The difference of JJA mean vertical velocity at 500 hPa between LGME and piControl
664 (in shading) and the corresponding climatology derived from piControl (yellow contours). The
665 thick black lines denote the coastal lines in LGME, and the thin black lines denote the coastal
666 lines in piControl. Only those areas where signal-to-noise ratio exceeds one are plotted in the
667 difference pattern.

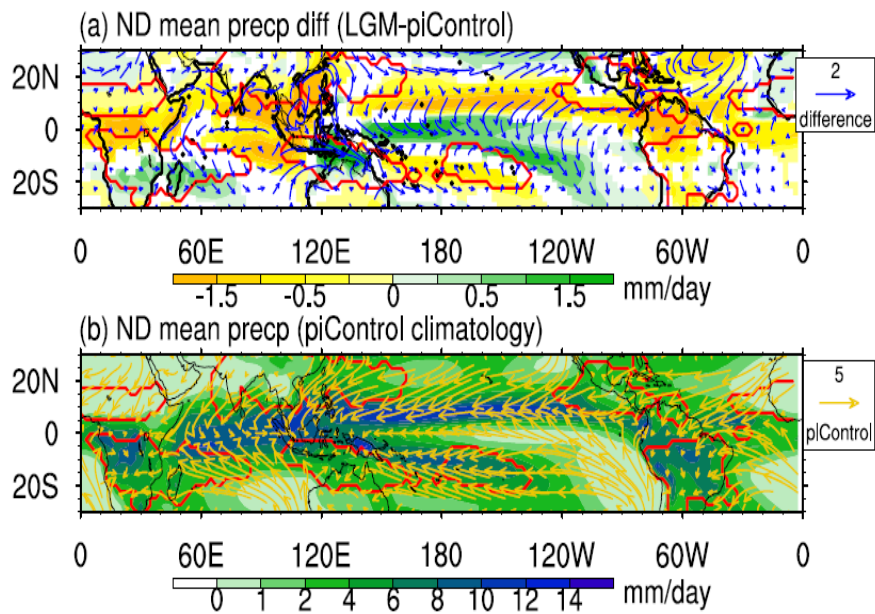
668



669

670 **Figure 5** JJA mean (a) surface air temperature, (b) sea level pressure (shading) with 850 hPa
 671 wind (vector), and (c) 850 hPa divergence differences between LGME and piControl. The red
 672 lines in (a) and (b) enclose the monsoon domains. The orange lines in (c) represent the
 673 climatology derived from piControl. The thick black lines denote the coastal lines in LGME, and
 674 the thin black lines denote the coastal lines in piControl. Only those areas where signal-to-noise
 675 ratio exceeds one are plotted.

676

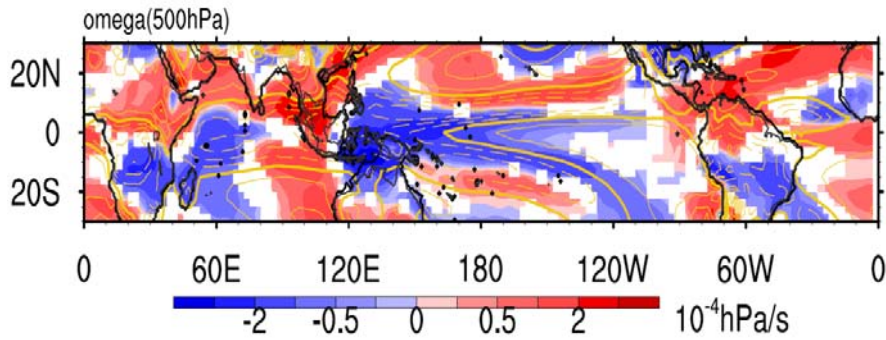


677

678 **Figure 6** (a) ND mean precipitation (shading) difference and surface wind (vectors) difference
 679 between LGME and piControl, and (b) the climatology of ND mean precipitation (shading) and
 680 surface wind (vectors) derived from piControl. The red lines enclose the monsoon domains. The
 681 thick black lines in (a) denote the coastal lines in LGME, and the thin black lines denote the
 682 coastal lines in piControl. Only those areas where signal-to-noise ratio exceeds one are plotted in
 683 (a).

684

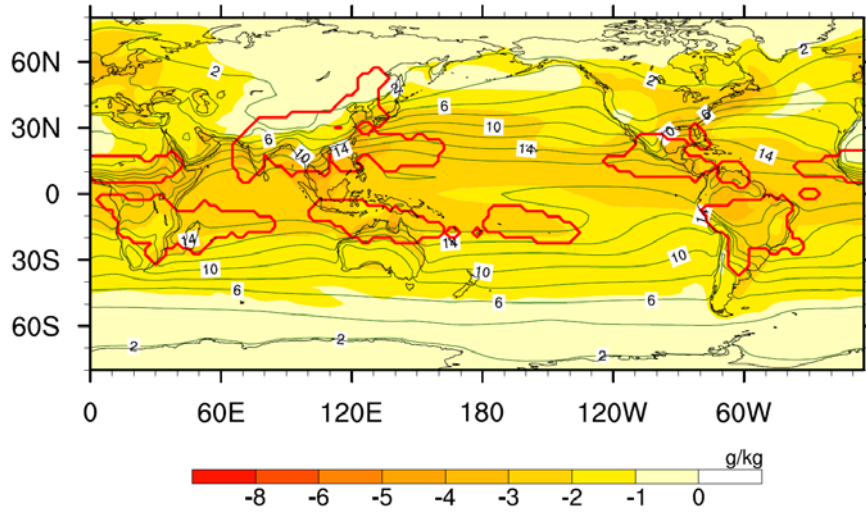
685



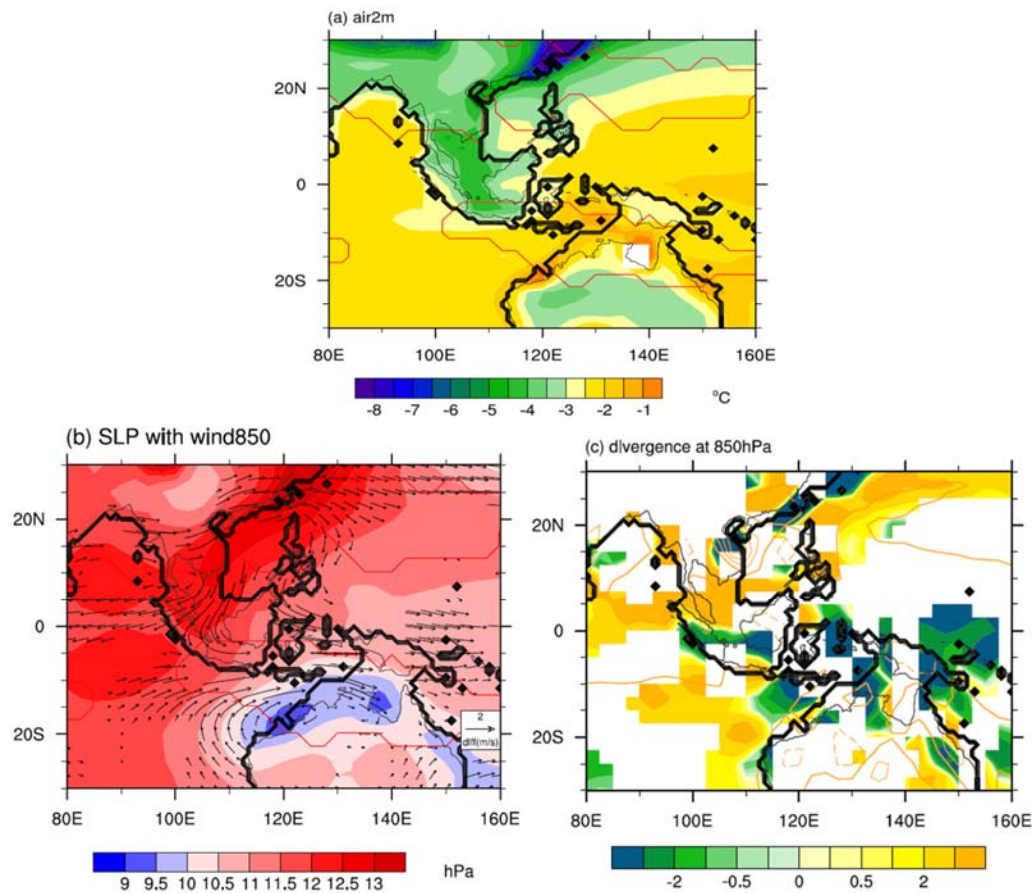
686

687 **Figure 7** The difference of the ND mean vertical velocity at 500 hPa between LGME and
688 piControl (in shading) and the corresponding climatology derived from piControl (yellow
689 contours). The thick black lines denote the coastal lines in LGME, and the thin black lines denote
690 the coastal lines in piControl. Only those areas where signal-to-noise ratio exceeds one are
691 plotted in the difference pattern.

692



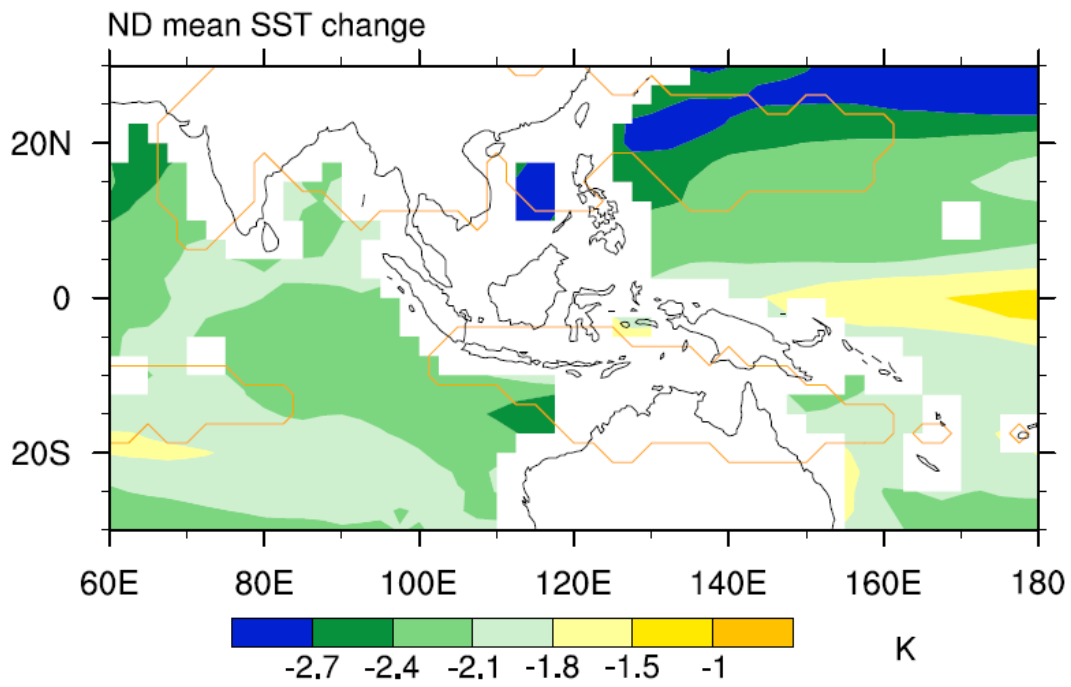
693 **Figure 8** Difference of ND mean surface specific humidity between LGME and piControl
 694 (shaded). The green contours denote the climatology derived from piControl. The red lines
 695 enclose the monsoon domains. Only those areas where signal-to-noise ratio exceeds one are
 696 plotted.
 697
 698



699

700 **Figure 9** ND mean (a) surface air temperature, (b) sea level pressure (shading) with 850 hPa
 701 wind (vector), and (c) 850 hPa divergence difference between LGME and piControl (shading).
 702 The red lines in (a) and (b) enclose the monsoon domains. The orange lines in (c) represents the
 703 climatology derived from piControl. The thick black lines denote the coastal lines in LGME, and
 704 the thin black lines denote the coastal lines in piControl. Only those areas where signal-to-noise
 705 ratio exceeds one are plotted.

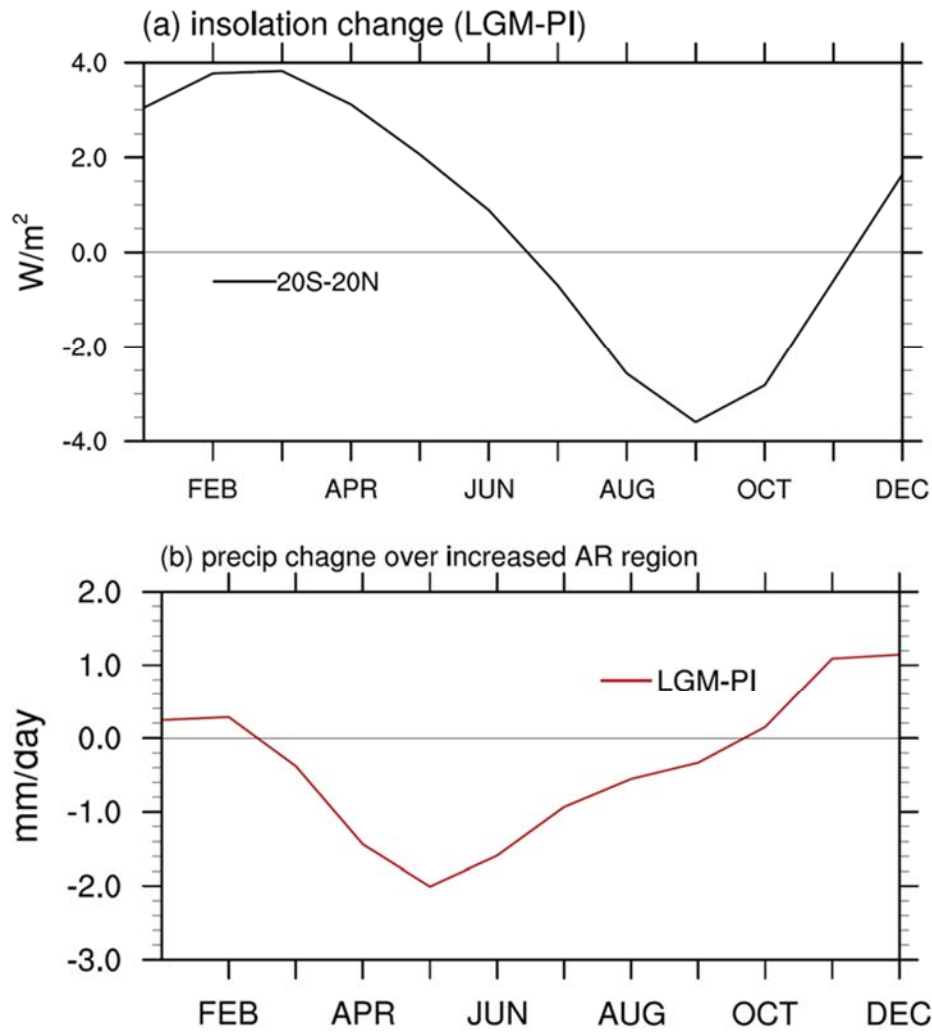
706



707

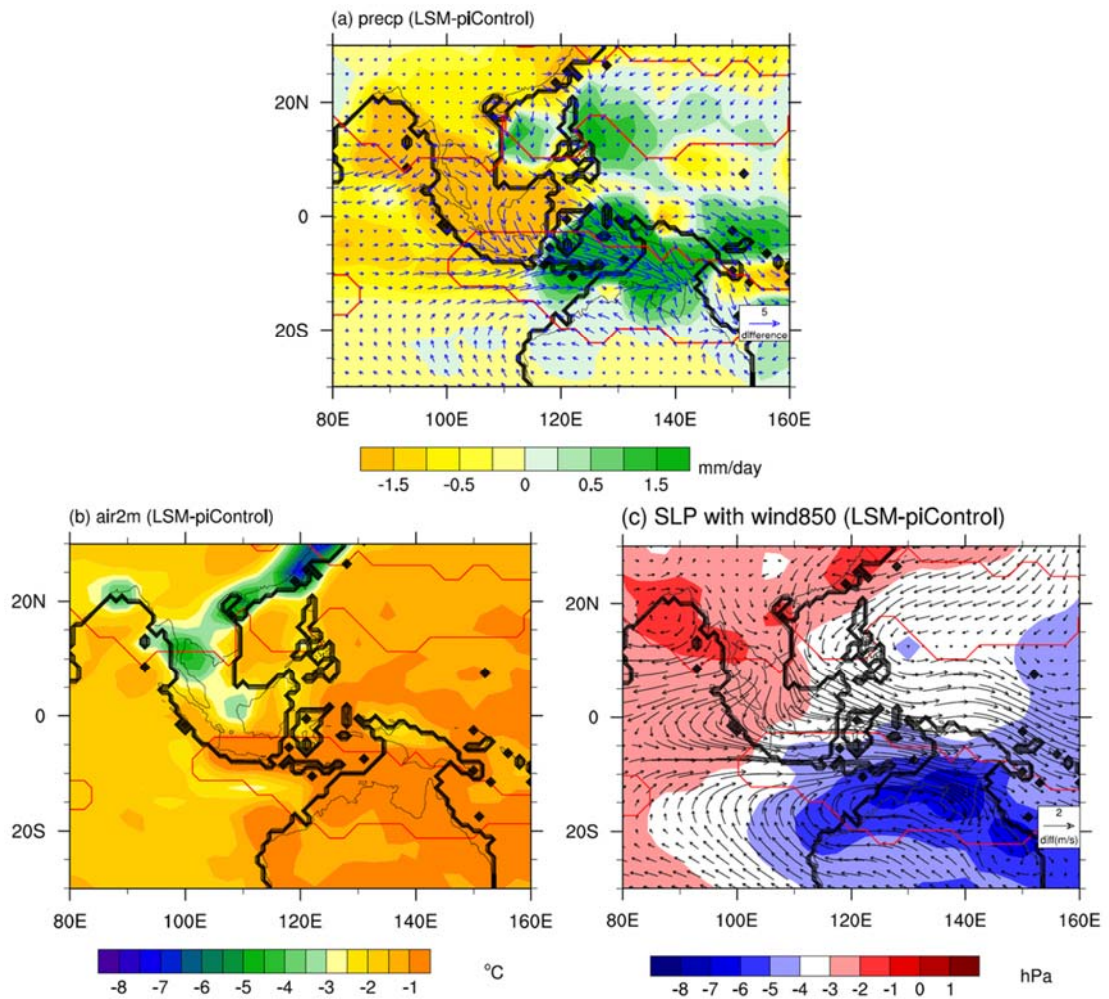
708 **Figure 10** ND mean SST difference between LGME and piControl. The red lines enclose the
 709 monsoon domains. Only those areas where signal-to-noise ratio exceeds one are plotted.

710



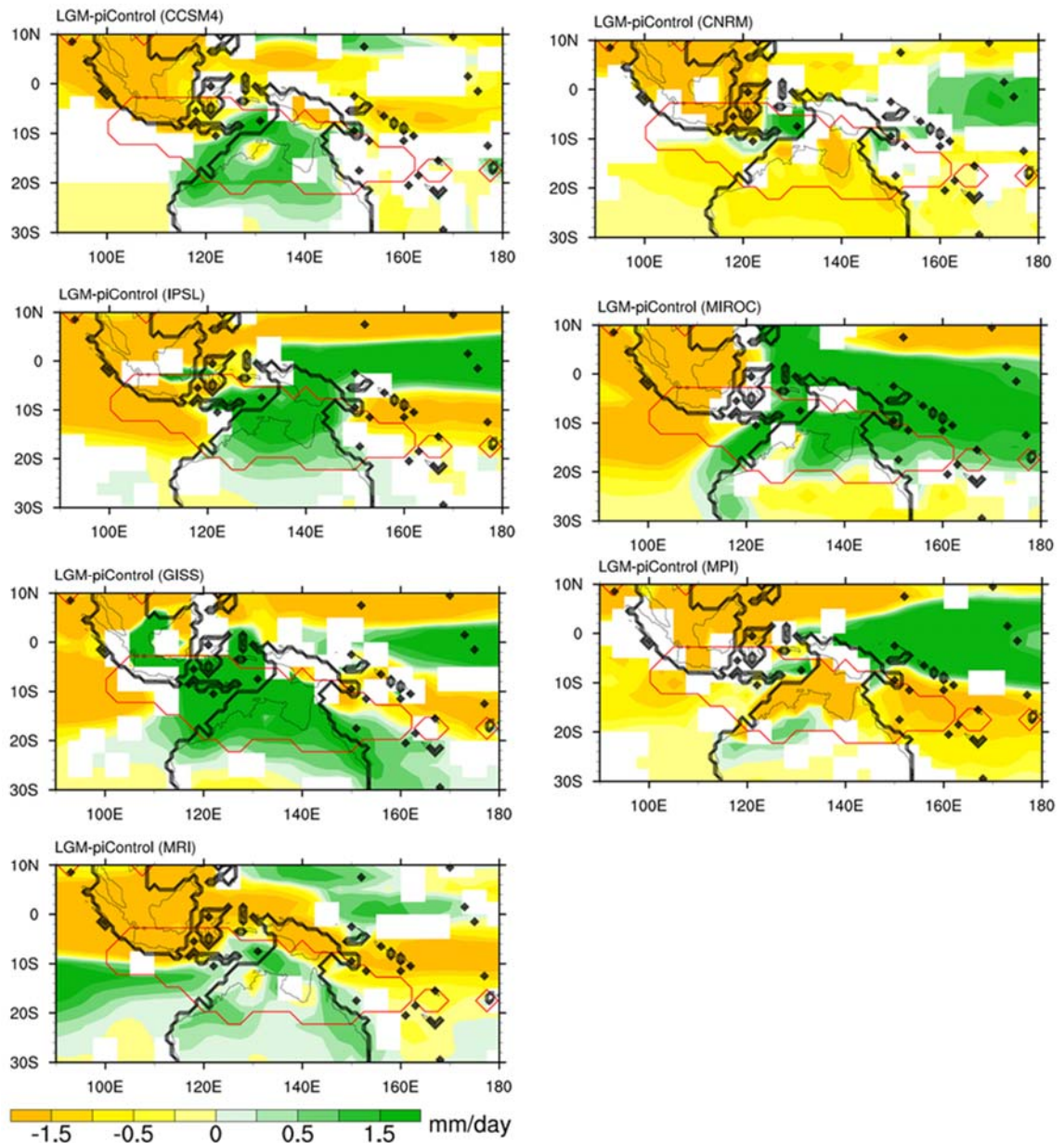
711
 712 **Figure 11** Seasonal distribution of (a) insolation change between 20°S and 20°N, and (b)
 713 precipitation change over the increased AR region as indicated in Fig. 1b (20°S-5°S, 120°E-
 714 145°E). The changes are calculated by the LGM value minus the PI value.

715
 716
 717
 718
 719
 720
 721



722

723 **Figure 12** ND mean (a) precipitation (shading) with 1000 hPa wind (vector), (b) surface air
 724 temperature, and (c) sea level pressure (shading) with 850 hPa wind (vector) difference between
 725 land sea configuration experiment (LSM) and piControl. The red lines enclose the monsoon
 726 domains. The thick black lines denote the coastal lines in LSM, and the thin black lines denote
 727 the coastal lines in piControl.



728

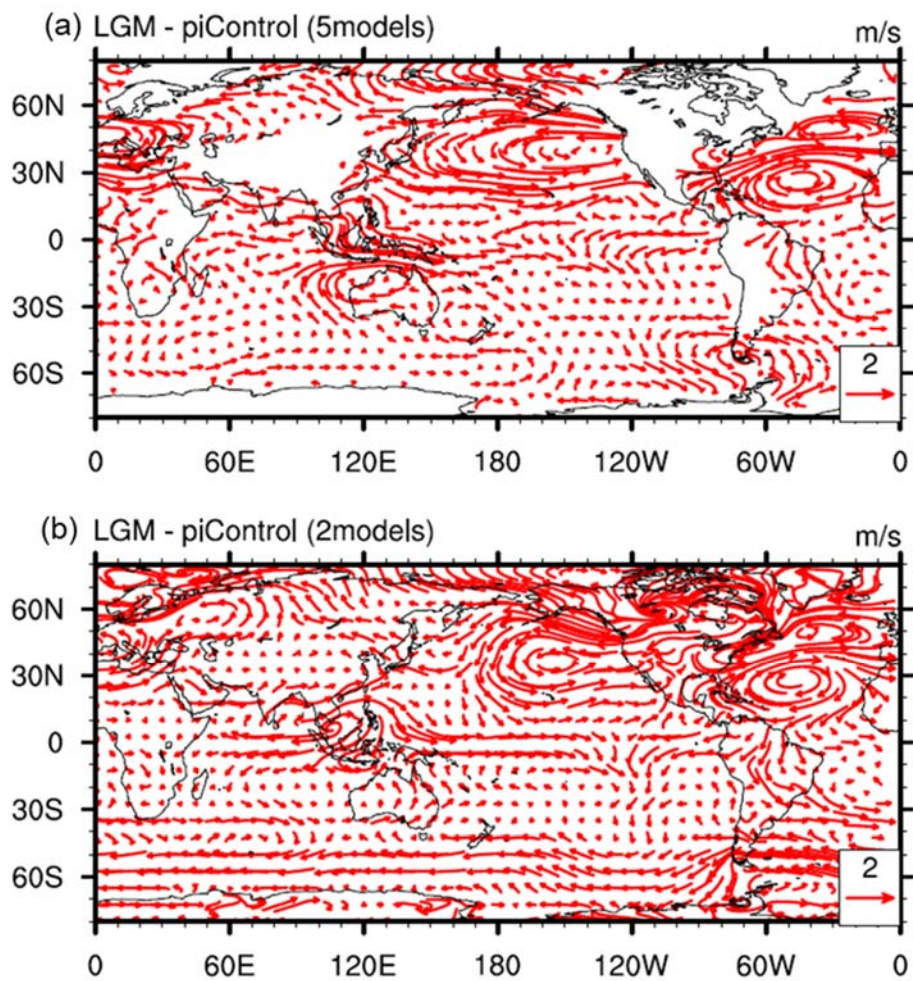
729 **Figure 13** DJF mean precipitation difference between LGME and piControl derived from each
 730 model. The red lines enclose the monsoon domains. Only those areas where signal-to-noise ratio
 731 exceeds one are plotted.

732

733

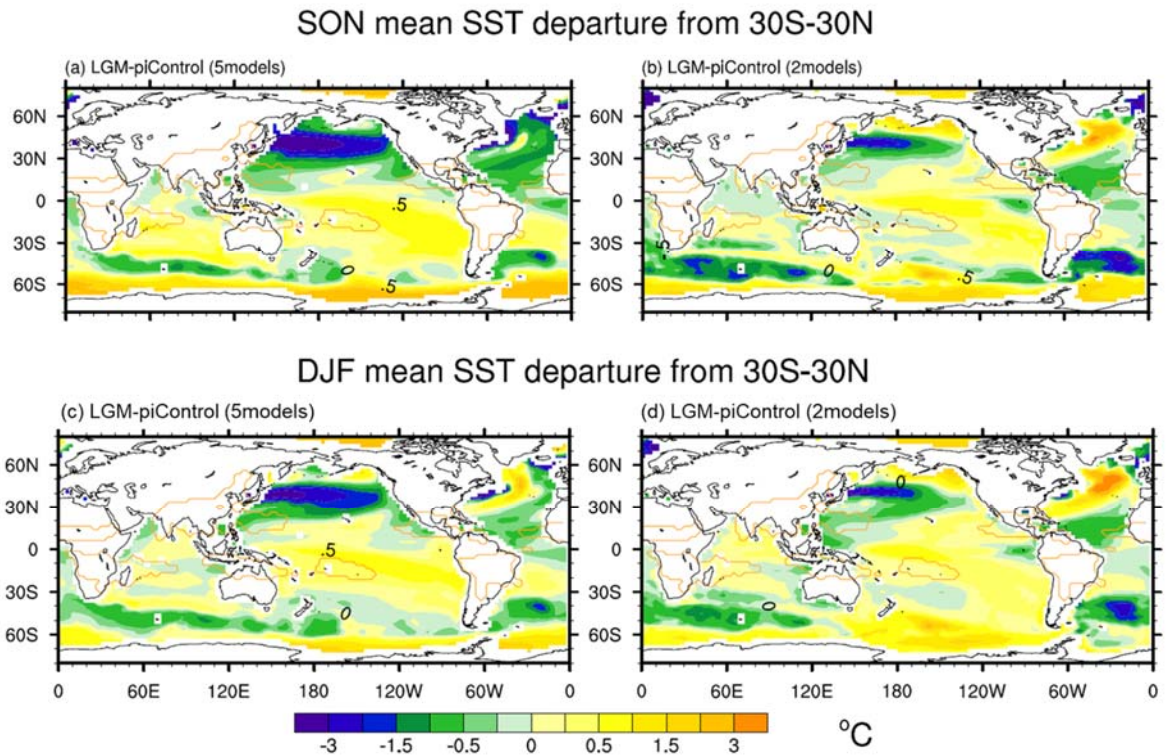
734

735



736
 737 **Figure 14** DJF mean 850hPa wind differences between LGME and piControl derived from (a)
 738 the five models and (b) the two models. Only those areas where signal-to-noise ratio exceeds one
 739 are plotted.

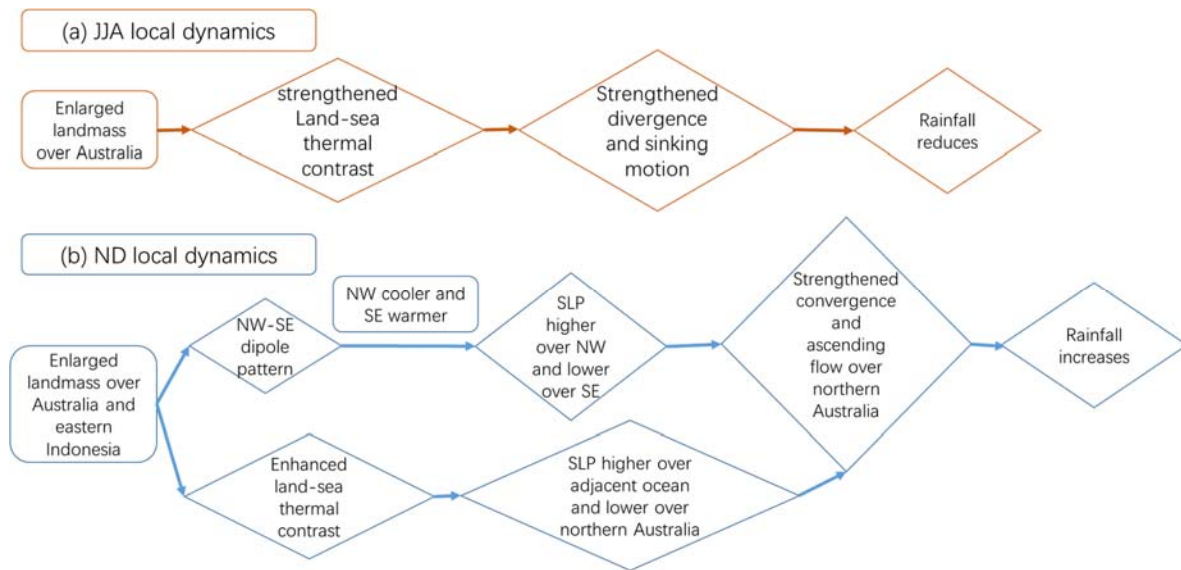
740



741
 742 **Figure 15** SON mean (a)-(b) and DJF mean (c)-(d) SST differences between LGME and
 743 piControl derived from (a), (c) the five models and (b), (d) the two models. Only those areas
 744 where signal-to-noise ratio exceeds one are plotted. The area average of tropical (30°S-30°N)
 745 SST change is distracted to make it clearer to illustrate the regional differences.
 746

747

748



749

750 **Figure 12** Mechanisms of Australian monsoon precipitation change (a) in JJA, and (b) in ND

751 during the LGM, in the local dynamics perspective.

752

753

754

755 **Table 1** CMIP5/PMIP3 models and experiments used in this study.

Model	Institution	piControl Time span (years)	LGME Time span (years)	Spatial resolution for atmospheric module Lon × Lat Grids	Spatial resolution for oceanic module Lon × Lat Grids
CCSM4	National Centre for Atmospheric Research (NCAR)	501	101	288 × 192	320×384
CNRM- CM5	Centre National de Recherches Meteorologiques/Centre Europeen de Recherche et Formation Avancees en Calcul Scientifique (CNRM-CERFACS)	850	200	256 × 128	362×292
GISS-E2-R	NASA Goddard Institute for Space Studies (NASA GISS)	1200	100	144 × 90	288×180
IPSL- CM5A-LR	Institute Pierre-Simon Laplace (IPSL)	1000	200	96 × 95	182×149
MIROC- ESM	Atmosphere and Ocean Research Institute, University of Tokyo, National Institute for Environmental studies, and Japan Agency for Marine-Earth Science and Technology	531	100	128 × 64	256×192
MPI-ESM- P	Max Planck Institute for Meteorology	1156	100	196 × 98	256×220
MRI- CGCM3	Meteorological Research Institute (MRI)	500	100	320 × 160	364×368

756
757

758

759 **Table 2** Main changed boundary conditions used for the piControl and LGME experiments.

	piControl	LGME
Orbital parameters	Eccentricity = 0.016724 Obliquity = 23.446° Angular precession = 102.04°	Eccentricity = 0.018994 Obliquity = 22.949° Angular precession = 114.42°
Trace gases	CO ₂ = 280 ppm CH ₄ = 650 ppb N ₂ O = 270 ppb	CO ₂ = 185 ppm CH ₄ = 350 ppb N ₂ O = 200 ppb
Ice sheets	Modern	Provided by ICE-6G v2 (Peltier, 2009)
Land surface elevation and coastlines	Modern	Provided by PMIP3

760

761

762

763 Table 3 Annual mean, austral summer (DJF) mean and annual range of precipitation change over
764 the region of (20°S-5°S, 120°E-145°E). The area averaged value is calculated based on the
765 areas where S2N ratio exceed one.

Model	Annual mean (mm/day)	Summer mean (mm/day)	Annual range (mm/day)
CCSM4	-0.14	0.49	1.36
CNRM-CM5	-0.78	-0.74	0.12
GISS-E2-R	0.79	3.74	4.66
IPSL-CM5A-LR	-0.17	0.90	1.82
MIROC-ESM	-0.53	1.25	3.17
MPI-ESM-P	-1.02	-1.71	-0.52
MRI-CGCM3	-0.68	-0.01	0.85
7MME	-0.36	0.56	1.61

766